



Steady State and Dynamic
Monoethanolamine (MEA) Test Runs
Conducted by CCSI² at the National Carbon
Capture Center

October 6, 2017



This material was produced under the U.S. Department of Energy's Carbon Capture Simulation Initiative (CCSI), and copyright is held by the software owners: ORISE, LANS, LLNS, LBL, PNNL, CMU, WVU, et al. The software owners and/or the U.S. government retain ownership of all rights in the CCSI software and the copyright and patents subsisting therein. Any distribution or dissemination is governed under the terms and conditions of the CCSI Test and Evaluation License, CCSI Master Non-Disclosure Agreement, and the CCSI Intellectual Property Management Plan. No rights are granted except as expressly recited in one of the aforementioned agreements.

Table of Contents

| | |
|---|-----------|
| 1. Introduction..... | 4 |
| 2. CCSI Model Background..... | 5 |
| 2.1. Absorber Model (Deterministic) | 5 |
| 2.2. Stripper Model (Deterministic) | 9 |
| 2.3. Stochastic Model (Estimation of Confidence Intervals)..... | 11 |
| 3. 2017 Steady State Test Campaign | 13 |
| 3.1. Design of Experiments..... | 13 |
| 3.2. Additional Model Validation | 24 |
| 4. 2017 Dynamic Test Campaign | 26 |
| 4.1 Design of Experiments..... | 26 |
| 4.2 Dynamic Data Reconciliation and Parameter Estimation | 32 |
| 4. Conclusions..... | 34 |
| References | 36 |

List of Figures

| | |
|---|----|
| Figure 1. Schematic of proposed Bayesian DOE for MEA campaign at NCCC. | 5 |
| Figure 2. Effect of lean solvent flow rate on CO ₂ capture percentage in absorber with three beds and intercooling, with variable CO ₂ weight fraction in flue gas and fixed value of flue gas flow rate (2250 kg/hr). | 7 |
| Figure 3. Effect of lean solvent flow rate, flue gas flow rate, and lean solvent loading on CO ₂ capture percentage of absorber (CO ₂ weight percent in flue gas fixed at 15%). | 8 |
| Figure 4. Estimated ranges of liquid flow rate, for a given value of lean loading and 15 wt% CO ₂ in flue gas, for which CO ₂ capture percentage is constrained between 50-95%. Solid lines represent the ranges of liquid flow rate for which the requirement is met, and dashed lines are included to illustrate the overall constraint for liquid flow rate (Eq. 1a). | 9 |
| Figure 5. Sensitivity study in which the required reboiler duty to reduce the lean solvent loading to a given value is calculated as a function of rich solvent flow rate and CO ₂ loading. | 10 |
| Figure 6. Estimated width of 95% confidence intervals in absorber CO ₂ capture percentage as a function of lean solvent flow rate, flue gas flow rate, and lean loading. | 12 |
| Figure 7. Estimated width of 95% confidence intervals in absorber CO ₂ capture percentage as a function of lean solvent flow rate, flue gas flow rate, and lean loading. | 13 |
| Figure 8. Parity plot for comparison of CO ₂ capture percentage predicted by Aspen Plus® simulation and surrogate response surface model..... | 15 |
| Figure 9. Graphical comparison of first set of experiments for 2017 campaign (black dots) and 2014 campaign (red dots)..... | 17 |
| Figure 10. Parity plot for comparison of model prediction of CO ₂ capture percentage to experimental data, for operation with three beds and intercooling. | 18 |

Figure 11. Estimated marginal PDFs for prior (blue) and posterior (red) distributions of parameters updated in Bayesian inference with CO₂ capture percentage data. 19

Figure 12. Effect of incorporating absorber efficiency data into Bayesian estimation of mass transfer and hydraulics model parameters. Confidence intervals widths, as calculated by the surrogate absorber model, are shown for (A) grid of 448 points spread throughout input space and (B) points for which experimental data are collected. 20

Figure 13. Parity plot for CO₂ capture percentage in absorber (three beds with intercooling configuration) for complete set of NCCC data. 22

Figure 14. Estimated marginal PDFs for prior (red) and posterior (green) distributions of parameters for the second round of Bayesian DOE. 23

Figure 15. Effect of second iteration of Bayesian DOE on 95% confidence interval widths of CO₂ capture percentage. Confidence intervals widths, as calculated by the surrogate absorber model, are shown for (A) grid of 448 points spread throughout input space and (B) points for which experimental data are collected. 24

Figure 16. Parity plot for CO₂ capture percentage predicted by model and experimental data for cases in which absorber is operated with one or two beds. 26

Figure 17. Single PRBS signal. 28

Figure 18. Estimated response due to PRBS inputs. 28

Figure 19. PRBS experiment design. 29

Figure 20. Schroeder phased input experiment design. 31

Figure 21. Schroeder phased input response signal estimation. 32

Figure 22. Reconciled Schroeder phased input results. 33

Figure 23. Reconciled PRBS results. 34

List of Tables

Table 1. List of parameters included as parameter distributions in stochastic model. 11

Table 2. First set of cases selected for 2017 MEA test campaign at NCCC. 16

Table 3. Results of three beds with intercooling test for first test plan. 18

Table 4. Test plan for second round of sequential DOE. 21

Table 5. Experimental data for second round of sequential DOE. 21

Table 6. Results of one bed absorber test. 25

Table 7. Results of two bed absorber test. 25

Table 8. Pilot plant characteristic parameters. 30

1. INTRODUCTION

US Department of Energy's Carbon Capture Simulation for Industry Impact (CCSI²) is a collaboration among national laboratories, universities, and industrial organizations with the goal of accelerating technology development, demonstration, and deployment using computational tools and models [1]. One of the process models that has been developed under the auspices of CCSI is a model designed to serve as a definitive reference for benchmarking the performance of solvent-based carbon dioxide (CO₂) capture systems. For developing the model, various submodels (e.g. physical properties, mass transfer, hydraulic models) have been developed independently, with uncertainty quantification, and combined into an overall process model. The project described in this work seeks to incorporate this existing model into a framework in which the initial (prior) estimated uncertainty is used to design a test plan for a monoethanolamine (MEA) solvent campaign, and this plan is continuously updated as new experimental data are used to alter the model uncertainty estimate.

A previous test campaign (Summer 2014) was conducted for the MEA solvent system and used as a basis for validating the process model developed as a part of CCSI. This campaign was designed using a space-filling approach with consideration to the manipulated variables of interest (flow rates of solvent, flue gas, and reboiler steam). In addition to these manipulated variables, variation in the number of absorber beds and presence of intercooling is considered. The output space, however, was not considered in the selection of the test cases. As a result, a large amount of data was collected for absorber operation at very high CO₂ capture percentage (>99%), and this clustering could have been avoided if a preliminary model had been considered for planning the test run.

The major goal of this project is to leverage the existing model of the National Carbon Capture Center (NCCC) pilot plant for an MEA system, which will be referred to as the CCSI model, for use in designing a test campaign with an optimal set of runs. This is accomplished by a sequential Bayesian design of experiments (DOE), a process that is characterized by the use of prior information in the planning of an experiment [2]. To the best of our knowledge, such an approach has not been applied to a large-scale pilot plant test. A schematic of the proposed DOE for this test campaign is shown in Figure 1.

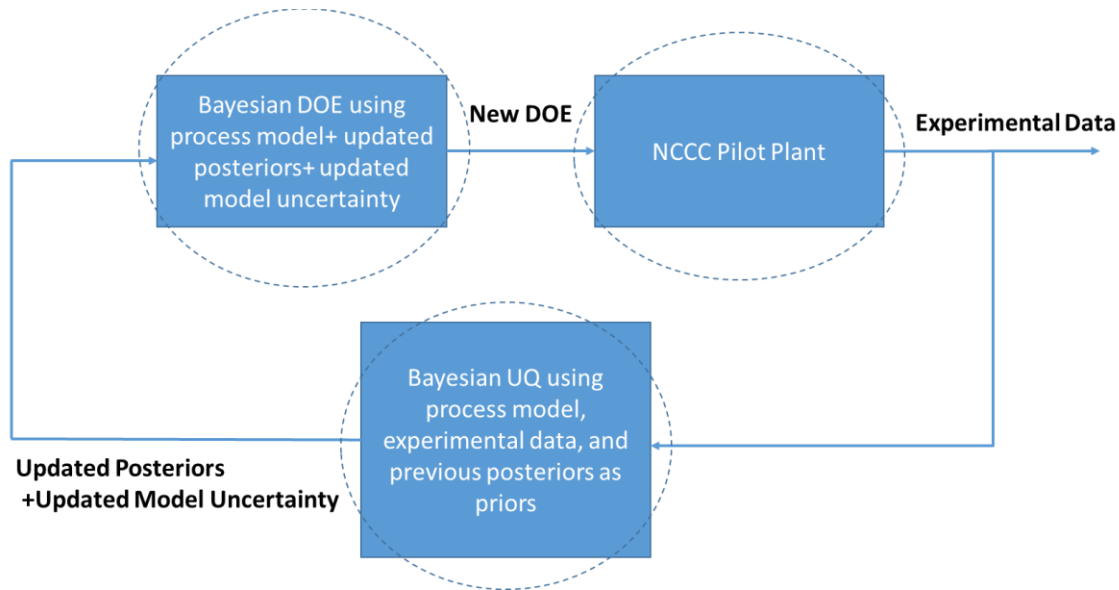


Figure 1. Schematic of proposed Bayesian DOE for MEA campaign at NCCC.

In this approach, an estimate of the uncertainty in the process model prediction of an output is generated prior to the planning stage of the experiment. The uncertainty in the CO₂ capture percentage in the absorber, considered to be the major output variable, is estimated by propagating the parametric uncertainty from the submodels of the process model (e.g. thermodynamic, mass transfer, and hydraulics model parameters). The DOE methodology is used to develop a test plan for experiments to be run at the NCCC pilot plant. The resulting experimental data are incorporated into a Bayesian inference methodology so that the distributions of some of the model parameters may be updated in light of the information provided by the new experimental data. As the model parameter distributions, and thus the estimation of the uncertainty in the model predictions, are updated as new experimental data are obtained, a new test plan may be developed.

2. CCSI MODEL BACKGROUND

2.1. Absorber Model (Deterministic)

In preparation for planning the test campaign, a rigorous analysis of the absorber operation over a wide range of operating conditions is performed for the CCSI MEA model, which has been validated satisfactorily with NCCC pilot plant data from the 2014 campaign. There are five possible test configurations for the absorber column at NCCC, given that the column consists of three beds, each separated by an intercooler. The configurations are three beds with and without intercooling, two beds with and without intercooling, and one bed without intercooling. As with the 2014 campaign, this work is focused on the three beds with intercooling process configuration due to the limitation in the amount of data that can be collected. A few data, however, are collected for the other process configurations so that the model's applicability with respect to packing height may be tested further. In this project, test

runs are planned with four major input variables: the lean solvent flow rate (L), flue gas flow rate (G), lean solvent loading (α_{lean}), and CO₂ weight fraction in the flue gas (w_{CO_2}). These variables are given the following constraints for this test campaign:

$$L \in [3000 - 13000] \text{ kg/hr} \quad (1a)$$

$$G \in [1000 - 3000] \text{ kg/hr} \quad (1b)$$

$$\alpha_{lean} \in [0.1 - 0.3] \text{ mol CO}_2/\text{MEA} \quad (1c)$$

$$w_{CO_2} \in [0.125 - 0.175] \quad (1d)$$

These ranges are based on the overall ranges for which data were given in the 2014 test campaign. Some of the previous data contain lean loading either above or below the range given here, although 0.3 mol CO₂/MEA has been determined to be a reasonable cut-off due to the high inefficiency of operating the absorber column at a higher loading. On the other hand, operation for lean loading below 0.1 mol CO₂/MEA would result in a very high reboiler duty requirement in the stripper column, and thus a high cost of operation. Since many of the test runs in the 2014 campaign gave absorber operation in the mass transfer-limited regime, with carbon capture higher than 99%, it is desired to select test runs for CO₂ capture percentage between 50-95% for this campaign. A sensitivity study is performed with the absorber model (three beds with intercooling) to quantify the CO₂ capture percentage as a function of the four input variables given in Eq. 1. An example of such a sensitivity study is given in Figure 2, in which CO₂ capture percentage is presented as a function of lean solvent flow rate and loading, as well as flue gas CO₂ weight fraction at a constant flue gas flow rate of 2250 kg/hr. For all work presented here, the nominal MEA weight fraction in solvent (on a CO₂-free basis) is set at 30%.

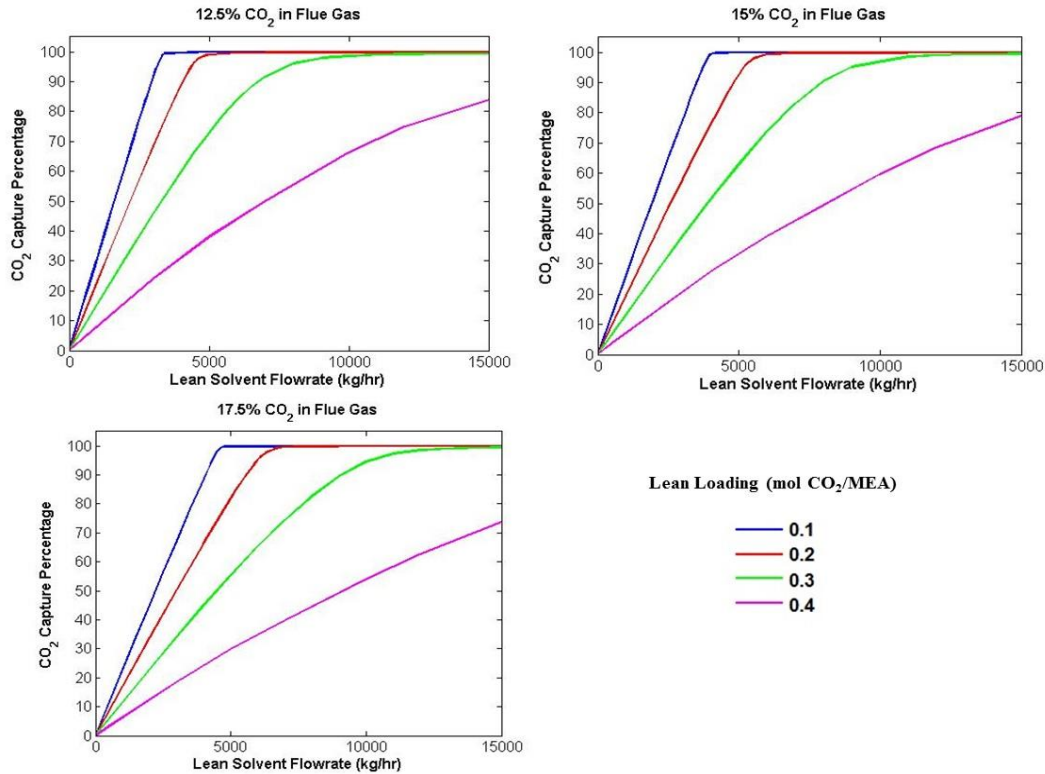


Figure 2. Effect of lean solvent flow rate on CO₂ capture percentage in absorber with three beds and intercooling, with variable CO₂ weight fraction in flue gas and fixed value of flue gas flow rate (2250 kg/hr).

For a given CO₂ loading in the solvent and CO₂ weight fraction in the flue gas, it is shown that the absorber efficiency increases approximately linearly with increasing solvent flow rate. At a sufficiently high flow rate, the capture percentage asymptotically approaches complete CO₂ capture with increasing flow rate. Since the column efficiency decreases with increasing CO₂ loading in the inlet solvent stream, the required liquid flow rate to reach complete CO₂ capture also increases monotonically with inlet solvent loading. Although 0.3 mol CO₂/MEA has been chosen as a cut-off point for this work, 0.4 mol CO₂/MEA is included in the figure to indicate the dramatic decrease in column efficiency that occurs at very high values of lean loading in the column. With all other variables held constant, the CO₂ capture percentage also decreases as the amount of CO₂ in the flue gas increases, although the sensitivity to this variable over the range of interest is relatively small in comparison to the other input variables.

Although the flue gas flow rate is fixed in Figure 2 at a common baseline value from the 2014 campaign, the model is also evaluated along a range of this variable. The sensitivity of the absorber CO₂ capture percentage to the flow rates of the lean solvent and flue gas flow rates are also shown for three distinct values of lean loading in Figure 3.

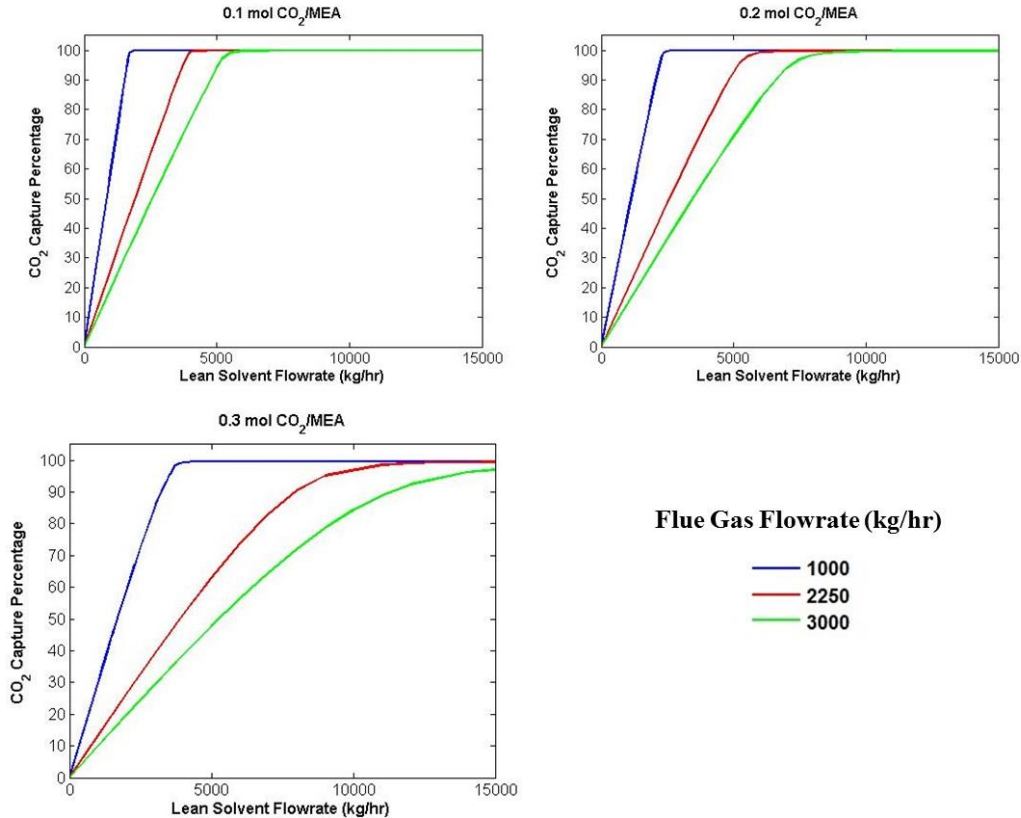


Figure 3. Effect of lean solvent flow rate, flue gas flow rate, and lean solvent loading on CO₂ capture percentage of absorber (CO₂ weight percent in flue gas fixed at 15%).

As expected, the CO₂ capture percentage decreases with increasing flue gas flow rate, as the amount of CO₂ to be captured also increases. The information provided from these sensitivity studies is used to constrain the range of liquid flow rate so that the estimated CO₂ capture percentage lies between 50-95%. These ranges are evaluated at discrete values of the remaining input variables, given by:

$$G \in [1000, 2250, 3000] \text{ kg/hr} \quad (2a)$$

$$\alpha_{lean} \in [0.1, 0.2, 0.25, 0.3] \text{ mol CO}_2/\text{MEA} \quad (2b)$$

$$w_{CO_2} \in [0.125, 0.15, 0.175] \quad (2c)$$

A trilinear interpolation procedure is used to estimate the upper and lower bounds of lean solvent flow rate over the entire ranges of interest of these variables (given in Eq. 1b-d). An example of the constraints on lean solvent flow rate is presented graphically in Figure 4. These results are given for 15 wt% CO₂ in flue gas; similar graphs have been generated for 12.5% and 17.5%, although these have been omitted for the purpose of brevity.

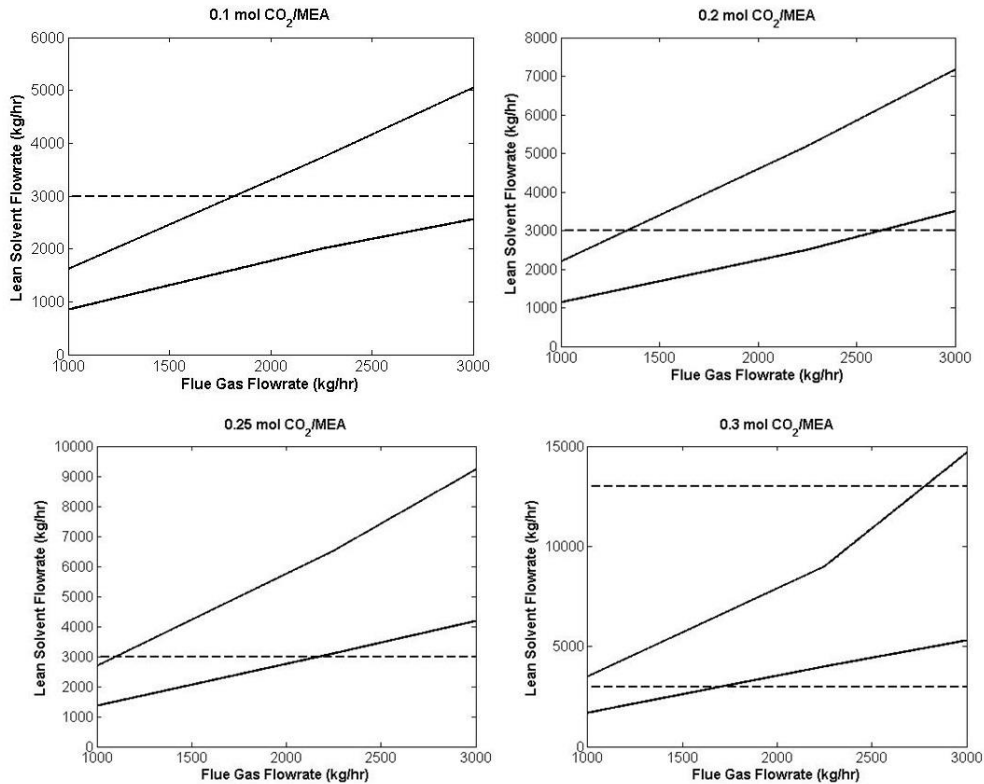


Figure 4. Estimated ranges of liquid flow rate, for a given value of lean loading and 15 wt% CO₂ in flue gas, for which CO₂ capture percentage is constrained between 50-95%. Solid lines represent the ranges of liquid flow rate for which the requirement is met, and dashed lines are included to illustrate the overall constraint for liquid flow rate (Eq. 1a).

As shown in Figure 4, the width of the range of lean solvent flow rate for which operation of the absorber column is considered desirable varies greatly with the other input variables. For example, at a low CO₂ loading (~ 0.1 mol CO₂/MEA), no cases would be chosen for a low flue gas flow rate (< 1700 kg/hr) because the entire solvent range for which the column operates between 50-95% efficiency lies below the minimum of 3000 kg/hr. On the other hand, a 95% capture condition would not be included for a high value of loading (~ 0.3 mol CO₂/MEA) and flue gas flow rate (~ 3000 kg/hr) because a solvent flow rate greater than the maximum of 13,000 kg/hr would be required. A similar, although less rigorous, procedure is used for the alternate process configurations, based on varying the number of absorber beds and the presence of intercooling, since some runs for these configurations are also desired to be included in the test run.

2.2.Stripper Model (Deterministic)

Although the design of the NCCC test plan is concerned primarily with the operation of the absorber column, some sensitivity analysis must also be performed for the stripper column. Although the lean solvent loading is considered as one of the input variables when designing the set of test runs, it is not directly manipulated as one of the plant variables, but it is dependent

on the input of steam to the reboiler in the stripper. The steam flow rate is directly proportional to the reboiler duty, which is considered here as a simulation input. The lean solvent loading may primarily be considered a function of the reboiler duty (\dot{Q}), rich solvent loading (α_{rich}), and rich solvent flow rate (\dot{m}_{rich}), of which the latter two are calculated as outputs of the absorber model. A sensitivity study for the required reboiler duty as a function of these input variables is given in Figure 5.

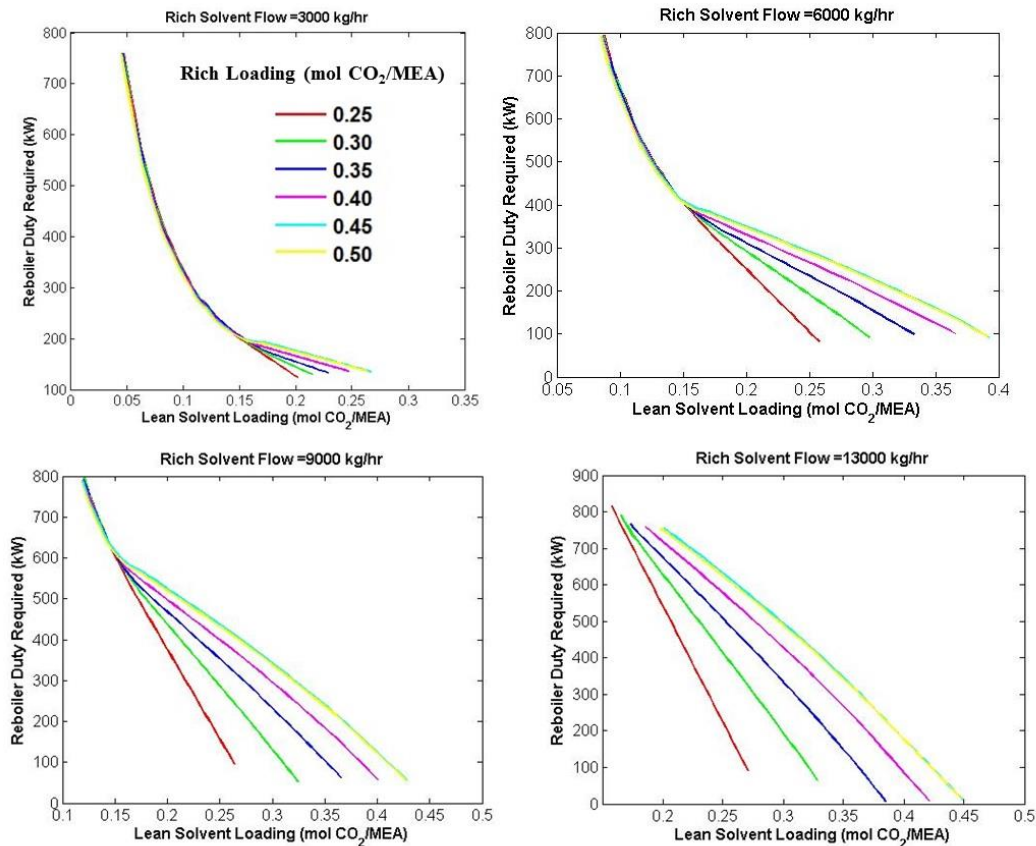


Figure 5. Sensitivity study in which the required reboiler duty to reduce the lean solvent loading to a given value is calculated as a function of rich solvent flow rate and CO₂ loading.

The reboiler duty requirement increases with increasing solvent flow rate and rich loading. As the outlet lean solvent loading approaches zero, the required reboiler duty becomes infinitely large, making operation at very low lean loading infeasible due to high operating costs associated with steam input requirement. It is shown that for a lean loading lower than a certain value (~ 0.15 mol CO₂/MEA), the reboiler duty requirement does not continue to decrease with a decrease in the rich solvent loading.

2.3. Stochastic Model (Estimation of Confidence Intervals)

The distributions of 13 parameters were propagated through the absorber model over a range of input variables of interest, including parameters for the thermodynamics, mass transfer, and hydraulic models. The thermodynamic model parameter distributions are estimated in our previous work [3], and the hydraulics and mass transfer model distributions will be presented in a future publication [4]. The deterministic parameter values are given in Table 1, and the parameter names correspond to the names provided in Aspen Plus®.

Table 1. List of parameters included as parameter distributions in stochastic model

| Parameter No. | Parameter Name | Deterministic Value |
|--------------------------------|----------------------------------|------------------------|
| Thermodynamic Model Parameters | | |
| 1 | DGAQFM (MEA+) [MJ/kmol] | -190 |
| 2 | DGAQFM (MEACOO-) [MJ/kmol] | -492 |
| 3 | DHAQFM (MEA+) [MJ/kmol] | -330 |
| 4 | DHAQFM (MEACOO-) [MJ/kmol] | -691 |
| 5 | HENRY/1 (MEA-H ₂ O) * | 28.6 |
| 6 | HENRY/2 (MEA-H ₂ O) | -7610 |
| 7 | NRTL/1 (MEA-H ₂ O) | 3.25 |
| 8 | NRTL/1 (H ₂ O-MEA) | 4.34 |
| 9 | NRTL/2 (H ₂ O-MEA) | -2200 |
| Mass Transfer Model Parameters | | |
| 10 | ARVAL/2 | 1.42 |
| 11 | DFACT/CO ₂ | 4.56×10^{-10} |
| Holdup Model Parameters | | |
| 12 | HURVAL/1 | 11.45 |
| 13 | HURVAL/2 | 0.647 |

* Henry constant parameters given corresponding to units of [Pa]

Results of propagating these parameter distributions through the absorber model are given in Figure 6. Estimates are given of the widths of the 95% confidence intervals for the absorber CO₂ capture percentage, calculated from estimates of the cumulative density functions (CDFs) of the values obtained from propagating the uncertainty through the model. Here, the confidence intervals widths are given as a function of the lean solvent and flue gas flow rates and solvent loading. The flue gas composition is fixed at 15 wt% CO₂, although the values are also calculated at other values. In this figure, squares are used to represent discrete points for which the confidence intervals are calculated, and lines are included to improve visibility of the trends.

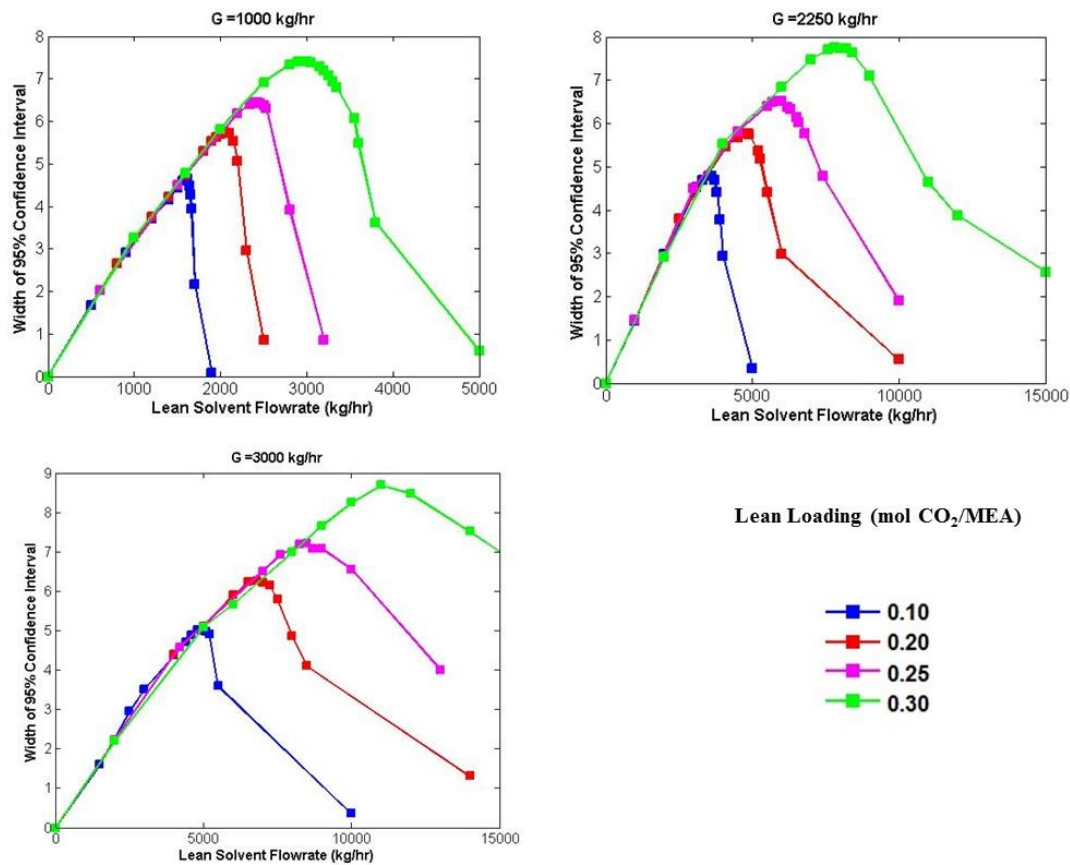


Figure 6. Estimated width of 95% confidence intervals in absorber CO₂ capture percentage as a function of lean solvent flow rate, flue gas flow rate, and lean loading.

With all other variables held constant, the amount of uncertainty in the CO₂ capture percentage is shown to increase approximately linearly with increasing lean solvent flow rate until reaching a maximum value, and decreases towards zero with further increase in the solvent flow rate. The maximum value of the confidence interval width, as well as the solvent flow rate at which it occurs, increases with increasing solvent CO₂ loading. Similar trends may be shown for variable CO₂ weight percentage in the flue gas. These trends are shown from another perspective in Figure 7, in which the confidence interval widths are given as a function of the CO₂ capture percentage instead of the lean solvent flow rate.

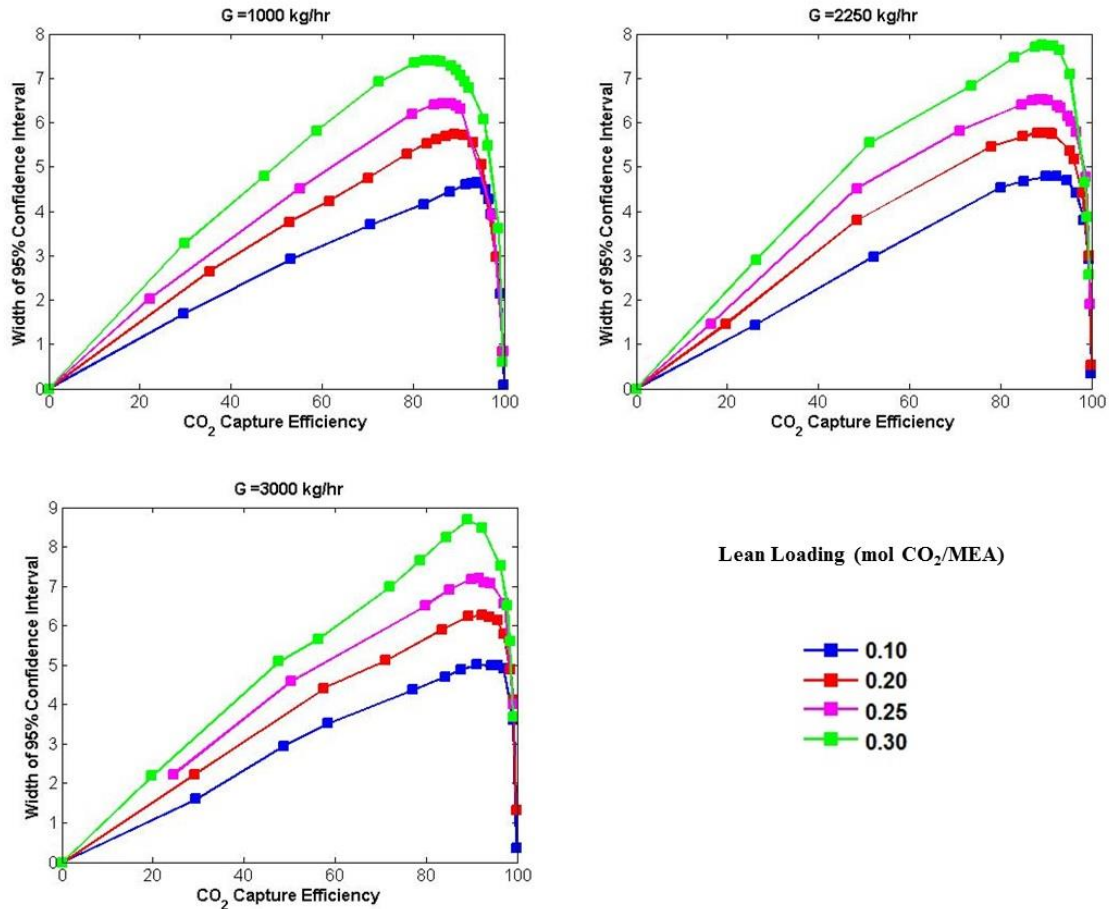


Figure 7. Estimated width of 95% confidence intervals in absorber CO₂ capture percentage as a function of lean solvent flow rate, flue gas flow rate, and lean loading.

From Figure 7, it is clear that the decrease in CO₂ capture percentage confidence interval width with further increase in lean solvent flow rate occurs at the point in which the column transitions between a reaction-limited regime and a mass transfer-limited regime at relatively high CO₂ capture. The application of the estimated confidence interval widths predicted by the stochastic absorber model to the Bayesian DOE is discussed in the following section.

3. 2017 STEADY STATE TEST CAMPAIGN

3.1. Design of Experiments

In the DOE methodology, the CO₂ capture percentage of the absorber column is represented by a surrogate model, which may be denoted as:

$$\hat{y} = \hat{y}(\tilde{x}, \tilde{\theta}_1, \tilde{\theta}_2) \quad (3)$$

The set of independent variables, which is defined in Eq. 1, is denoted as \tilde{x} , and \hat{y} refers to the response surface model prediction of the CO₂ capture percentage. The model parameters are divided into two groups; $\tilde{\theta}_1$ refers to the set of parameters of fixed uncertainty, and $\tilde{\theta}_2$ refers to the set of parameters for which the distributions are updated in this work considering the process data. The major rationale for considering two groups of parameters for this analysis is that the uncertainty of the physical property model parameters ($\tilde{\theta}_1$) have been adequately estimated from corresponding property data, and their uncertainty is independent of plant hardware. The distributions of the parameters for the mass transfer and hydraulics models ($\tilde{\theta}_2$), however, have been calibrated in previous work for bench-scale data that were not collected specifically for the packing type (MellapakPlus™ 252Y). Accordingly, the distributions of these parameters may be adjusted upon considering the process level data in a Bayesian framework. The response surface model is developed by simultaneously sampling from the parameter distributions (for both $\tilde{\theta}_1$ and $\tilde{\theta}_2$) and from the input variable space \tilde{x} . Due to some slight discrepancy in the planned test runs and the actual experimental data collected, the ranges of the CO₂ loading and the CO₂ weight fraction have been modified to encompass all experimental data. Essentially, Eq. 1 is replaced by:

$$L \in [3000 - 13000] \text{ kg/hr} \quad (4a)$$

$$G \in [1000 - 3000] \text{ kg/hr} \quad (4b)$$

$$\alpha_{lean} \in [0.1 - 0.35] \text{ mol CO}_2/\text{MEA} \quad (4c)$$

$$w_{CO_2} \in [0.1 - 0.175] \quad (4d)$$

For sampling the variables contained in \tilde{x} , a sample is taken from the uniform distribution of each of the four variables. Only points for which the value of L lies within the estimated ranges corresponding to a CO₂ capture percentage range of 50-95% are incorporated into the development of the response surface model. The estimated ranges for the liquid flow rate are determined by using the trilinear interpolation algorithm, as described previously in Section 2.1, which has been modified to be fully inclusive of the modified variable ranges in Eq. 4. A total of 5,773 observations are used for developing the response surface model, and the MARS method is used as described previously. A parity plot is given in Figure 8 to show the quality of the response surface as a surrogate for the actual model.

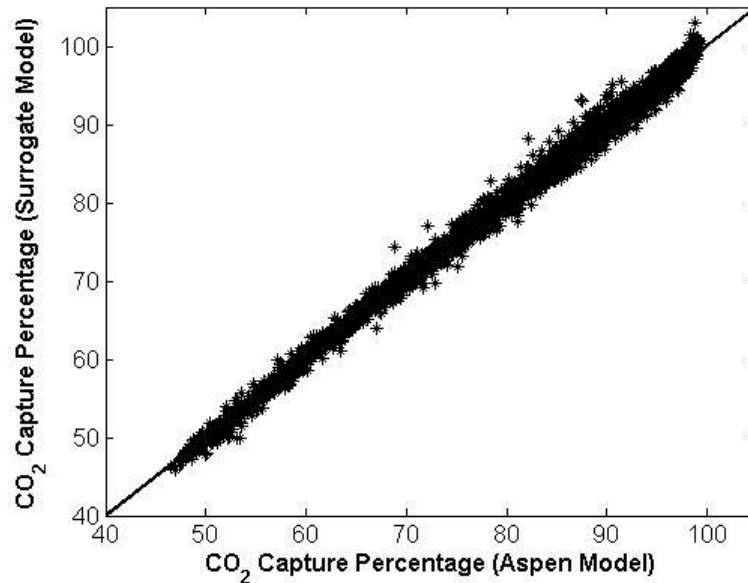


Figure 8. Parity plot for comparison of CO₂ capture percentage predicted by Aspen Plus[®] simulation and surrogate response surface model.

The response surface model developed using multivariate adaptive regression splines (MARS) has been shown to be an adequate surrogate for the actual absorber process model, and the correlation between the two models has been calculated as $R^2 \approx 0.995$.

The test cases have been chosen by a research collaborator, using an algorithm that involves a space-filling design that attempts to select points for which the confidence intervals, estimated as described in Section 2.3, are relatively wide. The test runs are selected from a grid of approximately 450 points, which covers the input variable values over the ranges described in Eq. 1, with the estimated CO₂ capture percentage constrained between 50-95% using the trilinear interpolation method discussed earlier. The final test plan, which includes 20 cases, is presented in Table 2.

Table 2. First set of cases selected for 2017 MEA test campaign at NCCC

| Case No. | Lean Solvent Flow Rate (kg/hr) | Flue Gas Flow Rate (kg/hr) | Lean Loading | Reboiler Steam Flow Rate (kg/hr) | Flue Gas CO ₂ Weight Fraction | CO ₂ Capture Percentage (Model Prediction) |
|----------|--------------------------------|----------------------------|--------------|----------------------------------|--|---|
| 1 | 3911 | 1250 | 0.3 | 251 | 0.175 | 77.3 |
| 2 | 3200 | 2250 | 0.25 | 261 | 0.14 | 54.8 |
| 3 | 3800 | 2500 | 0.15 | 438 | 0.1583 | 72.9 |
| 4 | 9384 | 3000 | 0.25 | 781 | 0.175 | 89.3 |
| 5 | 4171 | 3000 | 0.1 | 772 | 0.175 | 69.6 |
| 6 | 6817 | 2250 | 0.3 | 438 | 0.175 | 72.8 |
| 7 | 8186 | 3000 | 0.25 | 688 | 0.125 | 96.1 |
| 8 | 3133 | 1750 | 0.3 | 200 | 0.125 | 61.0 |
| 9 | 7946 | 3000 | 0.2 | 806 | 0.1583 | 97.3 |
| 10 | 3017 | 2750 | 0.1 | 558 | 0.1583 | 60.8 |
| 11 | 6514 | 2500 | 0.25 | 536 | 0.175 | 78.6 |
| 12 | 3609 | 3000 | 0.15 | 418 | 0.125 | 71.8 |
| 13 | 8024 | 2500 | 0.25 | 674 | 0.1583 | 96.3 |
| 14 | 9384 | 3000 | 0.25 | 781 | 0.175 | 89.3 |
| 15 | 3230 | 2250 | 0.1 | 597 | 0.175 | 72.3 |
| 16 | 6932 | 2750 | 0.2 | 692 | 0.175 | 90.2 |
| 17 | 4341 | 2000 | 0.2 | 430 | 0.1583 | 87.7 |
| 18 | 3360 | 1500 | 0.2 | 331 | 0.175 | 83.7 |
| 19 | 3370 | 2750 | 0.15 | 388 | 0.175 | 53.9 |
| 20 | 4734 | 2250 | 0.15 | 550 | 0.175 | 90.6 |

The estimated values of CO₂ capture given in Table 2 are calculated from the actual model instead of an approximation, so some of the values may be slightly above 95%. The final test plan for the first 20 runs is also displayed graphically in Figure 9.

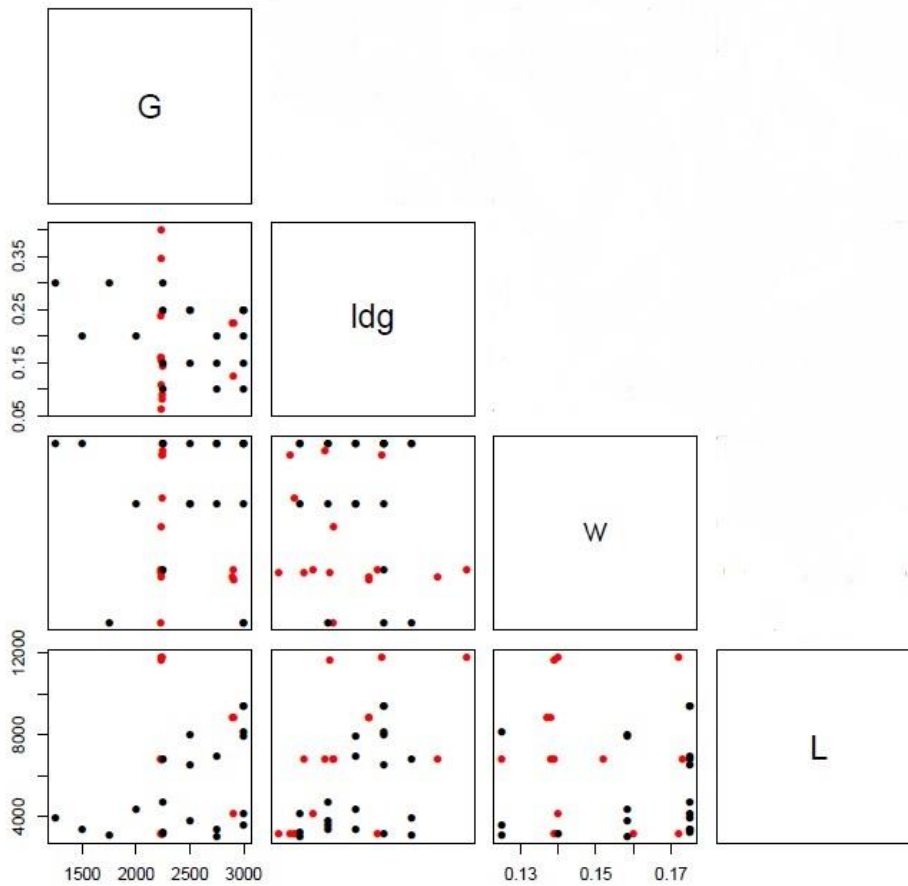


Figure 9. Graphical comparison of first set of experiments for 2017 campaign (black dots) and 2014 campaign (red dots).

Figure 9 shows the test points spread throughout the four-dimensional input space. The input variables and their planned ranges are defined in Eq. 1, and the variables ‘ldg’ and ‘w’ correspond to α_{lean} and w_{CO_2} , respectively. It should also be noted that only the data for the three beds with intercooling configuration, which comprise 15 of the 23 data points, are represented in this figure.

The final set of data incorporated into the first round of the parameter distribution updating is summarized in Table 3. The experimental data for CO₂ capture percentage are compared with model predictions, and the comparison is given in Figure 10.

Table 3. Results of three beds with intercooling test for first test plan

| Data No. | Lean Solvent Flow Rate (kg/hr) | Flue Gas Flow Rate (kg/hr) | Lean Solvent Loading (mol CO ₂ /MEA) | Flue Gas CO ₂ Fraction (weight) | CO ₂ Capture Percentage | |
|----------|--------------------------------|----------------------------|---|--|------------------------------------|-------|
| | | | | | Data | Model |
| 1 | 8180 | 3000 | 0.242 | 0.125 | 97.5 | 97.2 |
| 2 | 7130 | 2690 | 0.245 | 0.150 | 93.4 | 90.2 |
| 3 | 3354 | 1500 | 0.243 | 0.162 | 79.7 | 77.0 |
| 4 | 3600 | 3000 | 0.192 | 0.117 | 70.6 | 66.6 |
| 5 | 3380 | 2750 | 0.2 | 0.160 | 53.8 | 50.2 |
| 6 | 3130 | 1750 | 0.314 | 0.116 | 51.7 | 60.6 |
| 7 | 4730 | 2255 | 0.234 | 0.164 | 72.5 | 73.0 |
| 8 | 3230 | 2240 | 0.237 | 0.160 | 56.3 | 51.8 |
| 9 | 3224 | 2245 | 0.135 | 0.162 | 74.2 | 72.9 |
| 10 | 7980 | 2492 | 0.315 | 0.163 | 79.9 | 74.2 |
| 11 | 3016 | 2761 | 0.16 | 0.145 | 60.5 | 55.7 |
| 12 | 4170 | 2920 | 0.14 | 0.160 | 76.0 | 72.5 |
| 13 | 6910 | 2680 | 0.255 | 0.162 | 80.6 | 80.9 |
| 14 | 6505 | 2500 | 0.314 | 0.162 | 57.8 | 63.1 |
| 15 | 8000 | 2494 | 0.315 | 0.162 | 76.8 | 74.6 |

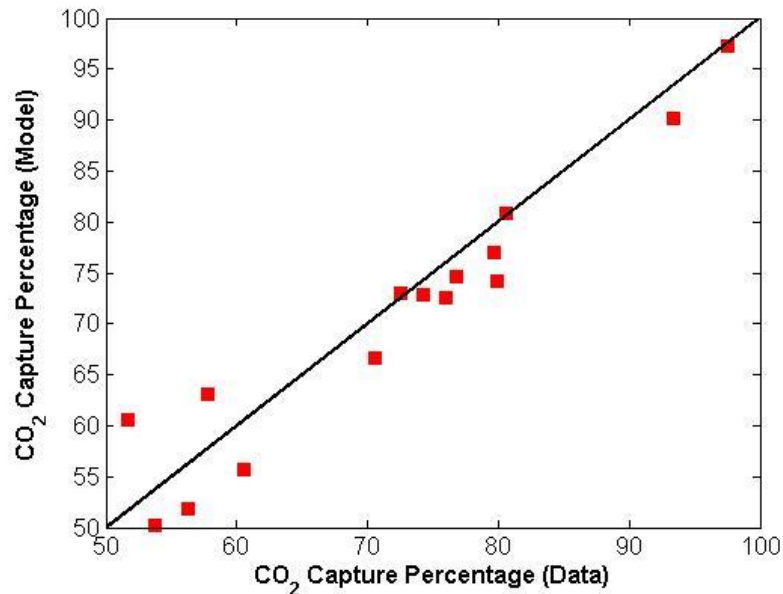


Figure 10. Parity plot for comparison of model prediction of CO₂ capture percentage to experimental data, for operation with three beds and intercooling.

These data are incorporated into a Bayesian inference methodology as follows. A sample from the distributions of parameters of fixed uncertainty $(\tilde{\theta}_1^{(1)}, \tilde{\theta}_1^{(2)}, \dots, \tilde{\theta}_1^{(j)}, \dots, \tilde{\theta}_1^{(n)})$ of size n is taken, and for each sample a posterior distribution of the parameters is $\tilde{\theta}_2$ is generated, which may be denoted as $\pi_j(\tilde{\theta}_2|Z, \tilde{\theta}_1^{(j)})$. The final posterior distribution $\pi(\tilde{\theta}_2|Z)$ is taken by combining all n of these distributions. A total of $n = 100$ iterations is used for this work. The change in the distributions of the four parameters contained in $\tilde{\theta}_2$ is shown in Figure 11. The parameter numbers were defined previously in Table 1.

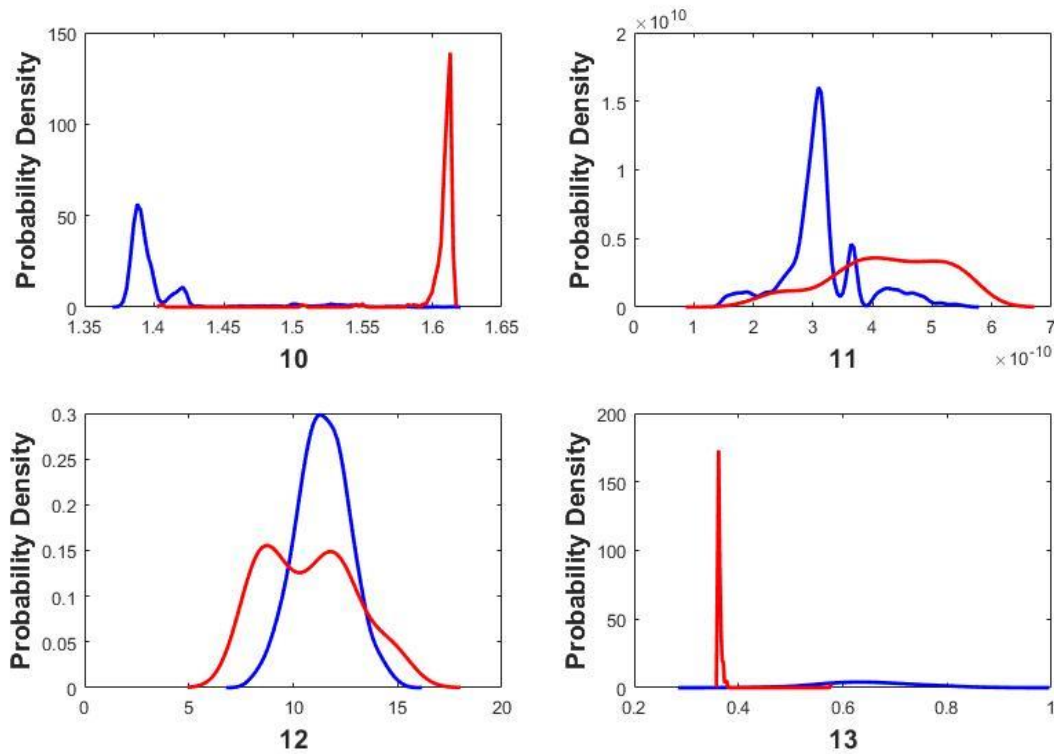


Figure 11. Estimated marginal PDFs for prior (blue) and posterior (red) distributions of parameters updated in Bayesian inference with CO₂ capture percentage data.

The values of parameters 10 and 13 are shifted as a result of the Bayesian inference, which may be attributed to the fact that the original values did not give the best fit of the model to the experimental data. The updated parameter distributions are used to determine the effect of incorporating the NCCC data into a Bayesian inference methodology to predict the updated model uncertainty, which is shown in Figure 12.

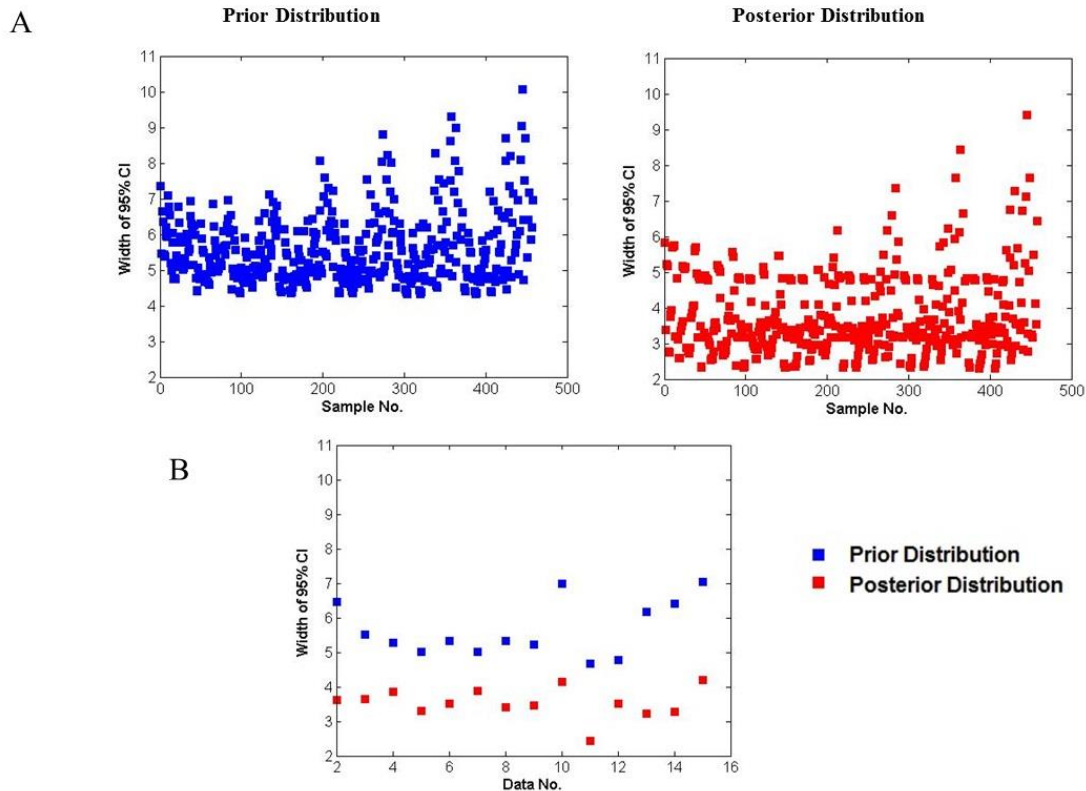


Figure 12. Effect of incorporating absorber efficiency data into Bayesian estimation of mass transfer and hydraulics model parameters. Confidence intervals widths, as calculated by the surrogate absorber model, are shown for (A) grid of 448 points spread throughout input space and (B) points for which experimental data are collected.

Note that the first data point is not included in Figure 12B due to the width of the confidence interval expanding due to inaccuracies in the response surface model at high CO₂ capture percentage values. Similarly, other points (11 out of 459 points considered) are not included in Figure 12A due to the same issue. As a result of incorporating the experimental data, the width of the confidence interval decreases by an average of 1.80 ± 0.65 for all of the points considered in the grid (shown in Figure 12A), and by an average of 2.12 ± 0.68 for the points for which data were collected (shown in Figure 12B). This highlights the effectiveness of the new experimental data, collected for test cases chosen from the Bayesian DOE, in reducing the uncertainty in the stochastic model prediction of CO₂ capture percentage. With the updated uncertainty values of CO₂ capture from the grid of 450 points, a new test run is designed and presented in Table 4. Note that only three points are included due to time constraints encountered during the execution of this project.

Table 4. Test plan for second round of sequential DOE

| Case No. | Lean Solvent Flow Rate (kg/hr) | Flue Gas Flow Rate (kg/hr) | Lean Loading (mol CO ₂ /MEA) | Reboiler Steam Flow Rate (kg/hr) | Flue Gas CO ₂ Weight Fraction | CO ₂ Capture Percentage (Model Prediction) |
|----------|--------------------------------|----------------------------|---|----------------------------------|--|---|
| 1 | 7971 | 2500 | 0.3 | 520 | 0.125 | 91.62 |
| 2 | 9881 | 2750 | 0.3 | 645 | 0.1417 | 91.28 |
| 3 | 11675 | 2750 | 0.3 | 761 | 0.175 | 90.76 |

For the updated test plan, it should be noted that all of the data are located in a regime close to complete CO₂ capture, which is likely a result of relatively high uncertainty in this region. The resulting data are given in Table 5. Note that the data values of CO₂ weight fraction were generally lower than the values given in the test plan, leading to higher values of CO₂ capture percentage than expected.

Table 5. Experimental data for second round of sequential DOE

| Data No. | Lean Solvent Flow Rate (kg/hr) | Flue Gas Flow Rate (kg/hr) | Lean Loading (mol CO ₂ /MEA) | Flue Gas CO ₂ Weight Fraction | CO ₂ Capture Percentage (Data) |
|----------|--------------------------------|----------------------------|---|--|---|
| 1 | 7959 | 2497 | 0.3 | 0.118 | 96.1 |
| 2 | 9871 | 2746 | 0.3 | 0.133 | 97.7 |
| 3 | 11412 | 2748 | 0.3 | 0.162 | 94.9 |

A final parity plot for all absorber data for the three beds with intercooling configuration from NCCC, including the 2014 campaign as well as both iterations of the 2017 campaign, is given in Figure 13.

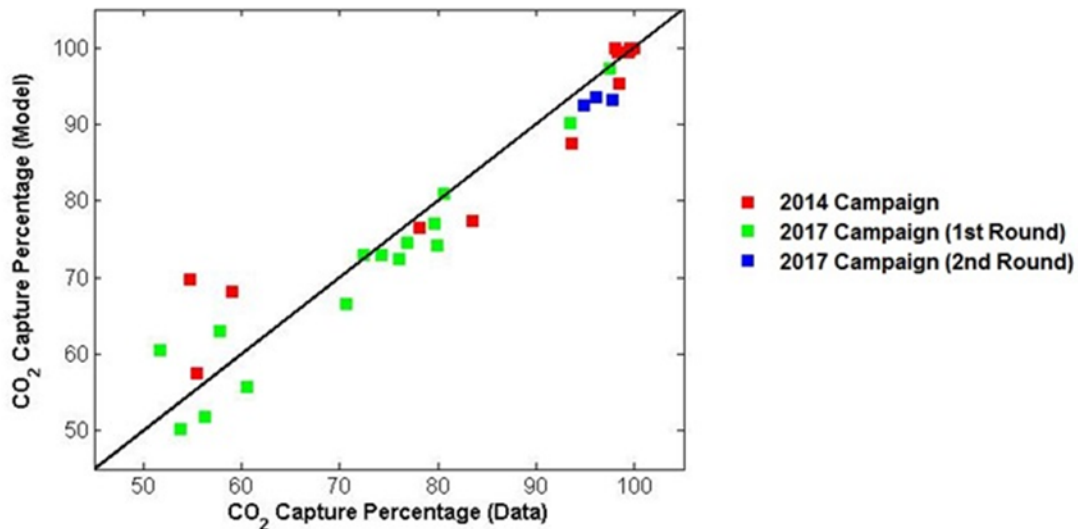


Figure 13. Parity plot for CO₂ capture percentage in absorber (three beds with intercooling configuration) for complete set of NCCC data.

As shown in Figure 13, the data for the 2017 campaign are widely spread over the range of CO₂ capture percentage of interest, especially in comparison to the 2014 campaign, in which many of the data are clustered at very high values of CO₂ capture. For the second round of the 2017 campaign, the data are located in a region (~ 95-98% CO₂ capture) in which the estimated uncertainty, calculated by propagating the submodel parametric uncertainty through the process model, is relatively high.

The data given in Table 5 are incorporated into a Bayesian inference framework, as described previously. The distribution of thermodynamic model parameters remains constant, and the distribution of mass transfer and hydraulic model parameters is updated, with the posterior given in Figure 11 used as the prior distribution for this round of uncertainty quantification. The estimated single parameter marginal prior and posterior distributions for the mass transfer and hydraulics model parameters are given, for the second round of Bayesian DOE, in Figure 14.

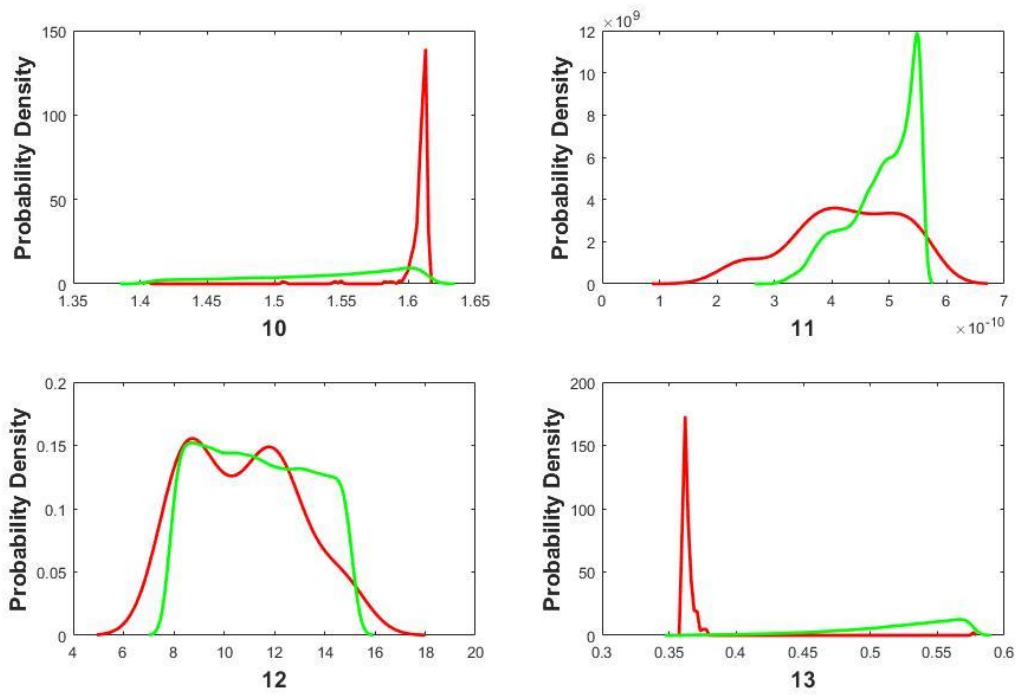


Figure 14. Estimated marginal PDFs for prior (red) and posterior (green) distributions of parameters for the second round of Bayesian DOE.

The corresponding change in the estimated values of the width of the 95% confidence intervals in CO₂ capture percentage for the data points is given in Figure 15.

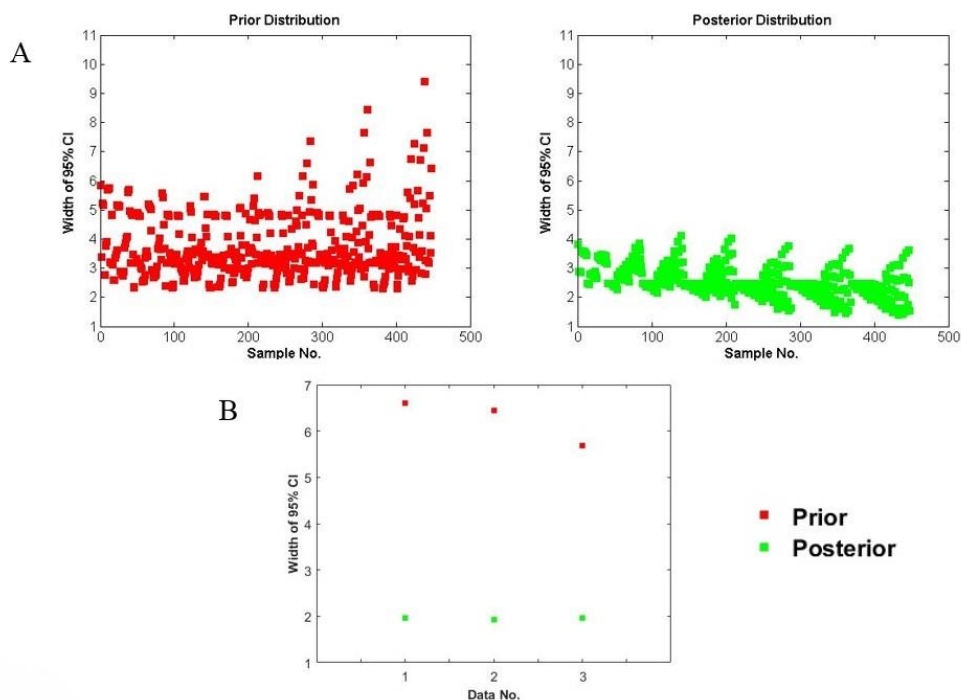


Figure 15. Effect of second iteration of Bayesian DOE on 95% confidence interval widths of CO₂ capture percentage. Confidence intervals widths, as calculated by the surrogate absorber model, are shown for (A) grid of 448 points spread throughout input space and (B) points for which experimental data are collected.

The confidence intervals for the experimental conditions in which data were collected in the second round of Bayesian DOE are shown to decrease in width as a result of updating the parameter distributions. Due to time constraints, no further iterations of this process could be performed during the 2017 test campaign. Nevertheless, the applicability of the Bayesian DOE to the planning of a pilot plant test campaign has been demonstrated in this work.

3.2. Additional Model Validation

During the 2014 MEA campaign, very few data were obtained for absorber configurations other than three beds with intercooling, which may be considered as the default configuration. As these data are valuable for assessing the overall predictability of the absorber model, some effort has been made to include test runs other than those for the default configuration. Test runs with variable bed numbers are especially useful for determining the predictability with respect to the packing height of the absorber. The test runs collected for cases in which the absorber is operated with one and two beds are summarized in Tables 6-7, respectively. No intercooling was used between the beds for the two-bed operation in this case. These test runs have been selected from a space-filling algorithm, similar to that used for the default configuration, although the confidence intervals obtained from propagating the parametric uncertainty are not taken into consideration here. The final set of data collected is similar to the test plan, with some variation in the input variable values. Note that some of the values of

composition variables fall slightly outside the ranges defined for the test plan (0.1-0.3 mol CO₂/MEA for the lean solvent loading and 0.125-0.175 for flue gas CO₂ weight fraction), although this does not have a major impact on the quality of the data obtained. The quality of the model fit to experimental data is also shown in Figure 16 in the form of a parity plot.

Table 6. Results of one bed absorber test

| Data No. | Lean Solvent Flow Rate (kg/hr) | Flue Gas Flow Rate (kg/hr) | Lean Solvent Loading (mol CO ₂ /MEA) | Flue Gas CO ₂ Fraction (Weight) | CO ₂ Capture Percentage | |
|----------|--------------------------------|----------------------------|---|--|------------------------------------|-------|
| | | | | | Data | Model |
| 1 | 6185 | 1997 | 0.15 | 0.118 | 97.1 | 95.4 |
| 2 | 7765 | 2499 | 0.20 | 0.118 | 92.3 | 87.6 |
| 3 | 7517 | 2013 | 0.25 | 0.140 | 89.5 | 84.0 |
| 4 | 6160 | 1500 | 0.25 | 0.162 | 88.9 | 87.6 |
| 5 | 5237 | 1498 | 0.26 | 0.118 | 86.4 | 87.3 |
| 6 | 7665 | 2700 | 0.314 | 0.118 | 60.2 | 58.8 |
| 7 | 5414 | 1000 | 0.34 | 0.150 | 76.4 | 78.8 |

Table 7. Results of two bed absorber test

| Data No. | Lean Solvent Flow Rate (kg/hr) | Flue Gas Flow Rate (kg/hr) | Lean Solvent Loading (mol CO ₂ /MEA) | Flue Gas CO ₂ Fraction (weight) | CO ₂ Capture Percentage | |
|----------|--------------------------------|----------------------------|---|--|------------------------------------|-------|
| | | | | | Data | Model |
| 1 | 4912 | 1500 | 0.3 | 0.15 | 77.8 | 80.1 |
| 2 | 4600 | 2000 | 0.2 | 0.175 | 80.5 | 81.2 |
| 3 | 9534 | 2502 | 0.3 | 0.140 | 87.0 | 81.5 |
| 4 | 4733 | 1966 | 0.2 | 0.120 | 96.4 | 96.9 |

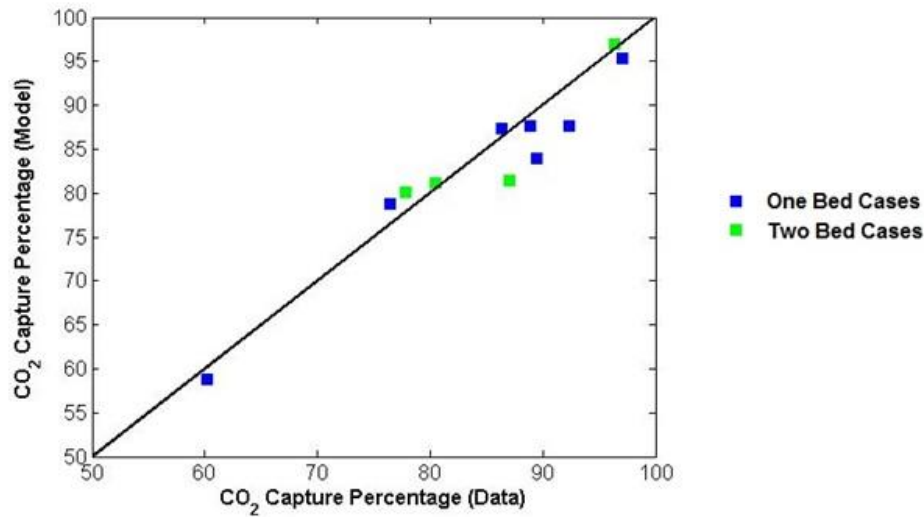


Figure 16. Parity plot for CO₂ capture percentage predicted by model and experimental data for cases in which absorber is operated with one or two beds.

The fit of the model to experimental data for absorber operation with one or two beds is shown to be reasonably accurate. This provides further insight of the predictability of the CCSI MEA model for the absorber column with variation in the packing height, especially considering that few runs were conducted for these configurations in the 2014 campaign.

4. 2017 DYNAMIC TEST CAMPAIGN

4.1 Design of Experiments

Similarly to the steady state campaign, the dynamic test run focused on key input variables that can be controlled during operation, such as the CO₂ weight fraction in the flue gas (w_{CO_2}) and the flow rates of lean solvent (L), flue gas (G) and reboiler steam (S). The range of each variable was defined taking into consideration process knowledge from NCCC engineers to ensure safety and stability during operation, these are presented below:

$$L \in [5390 - 5958] \text{ kg/hr} \quad (5a)$$

$$G \in [2136 - 2363] \text{ kg/hr} \quad (5b)$$

$$S \in [466 - 515] \text{ kg/hr} \quad (5c)$$

$$w_{CO_2} \in [0.1 - 0.175] \quad (5d)$$

Two different experiment designs were planned for the dynamic test campaign: a Pseudo-Random Binary Sequence (PRBS) and a Schroeder phased input. Both are classic approaches that can be used to generate rich data for multi-variable system identification or control design, while ensuring plant-friendliness constraints, such as 1) including output deviations low, 2) implementing short duration signals and 3) keeping move sizes small (Rivera et al., 2009).

The implementation of the methodology can be summarized by four steps:

- Plant information gathering/estimation
- Generation of input signal
- Signal optimization for plant-friendliness
- Response signal analysis (optional)

The dynamic model released as part of the CCSI toolset was used to represent the NCCC pilot plant, including buffer and storage tanks, and was applied in plant information estimation and the response signal analysis steps. The value of having a high-fidelity model prior to the experiment design becomes apparent in these steps as no preliminary tests are required for obtaining information on the highest and lowest dominant time constants (τ_{dom}^H and τ_{dom}^L) of the pilot plant and other characteristic parameters that are used to design the test runs. Additionally, the model can be used to verify the response signal of the pilot plant, ensuring that the plant-friendliness constraints are held.

The input signal is generated differently for each of the approaches, the PRBS design varies between the upper and lower bounds of the key variables, with a number of signals N_S defined as:

$$N_S = 2^{n_r} - 1 \geq \frac{2\pi\beta_S\tau_{dom}^H}{T_{sw}} \quad (6)$$

where, n_r is the number of input variables.

With four input variables, it is necessary to consider a delay D between the start of each subsequent signal after the first. The delay is defined as:

$$D = \frac{T_{settle}^{max}}{T_{sw}} \quad (7)$$

with the switching time T_{sw} being defined as:

$$T_{sw} = \frac{2.8\tau_{dom}^L}{\alpha_S} \quad (8)$$

A summary of the pilot plant information parameters is presented in Table 8. It is worth noting that all four signals are equivalent, only being shifted by the time delay D . Figure 17 presents

the generated signal. Although the resulting signal either has a value of +1 or -1, the magnitude can be defined to ensure plant-friendliness. Figure 18 presents the estimated response signal obtained from the process model and Figure 19 its corresponding inputs.

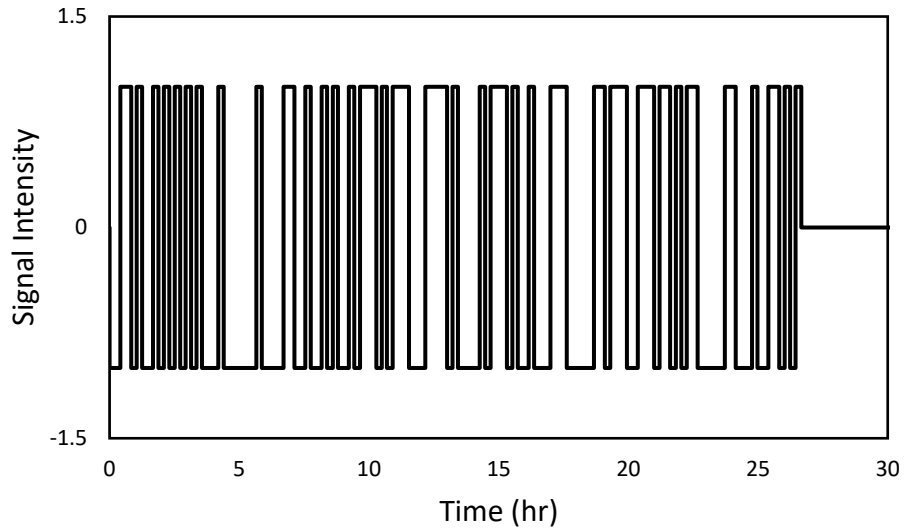


Figure 17. Single PRBS signal

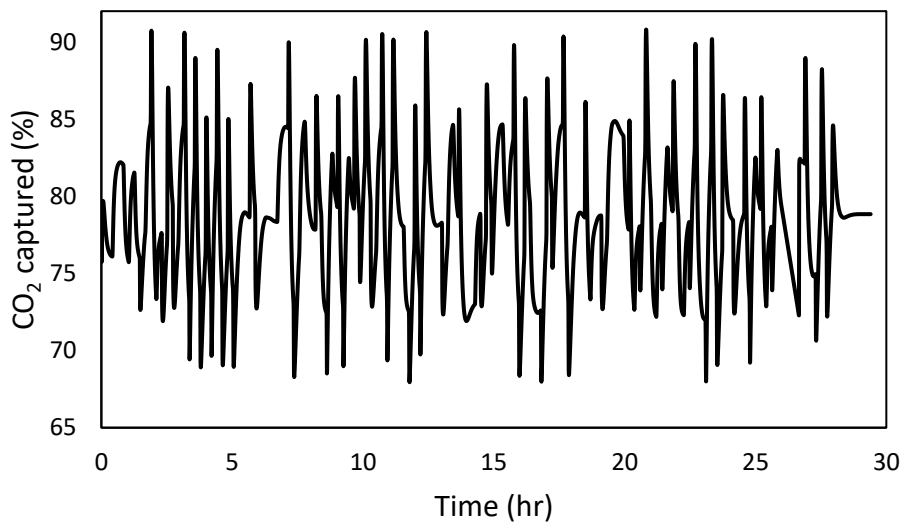


Figure 18. Estimated response due to PRBS inputs

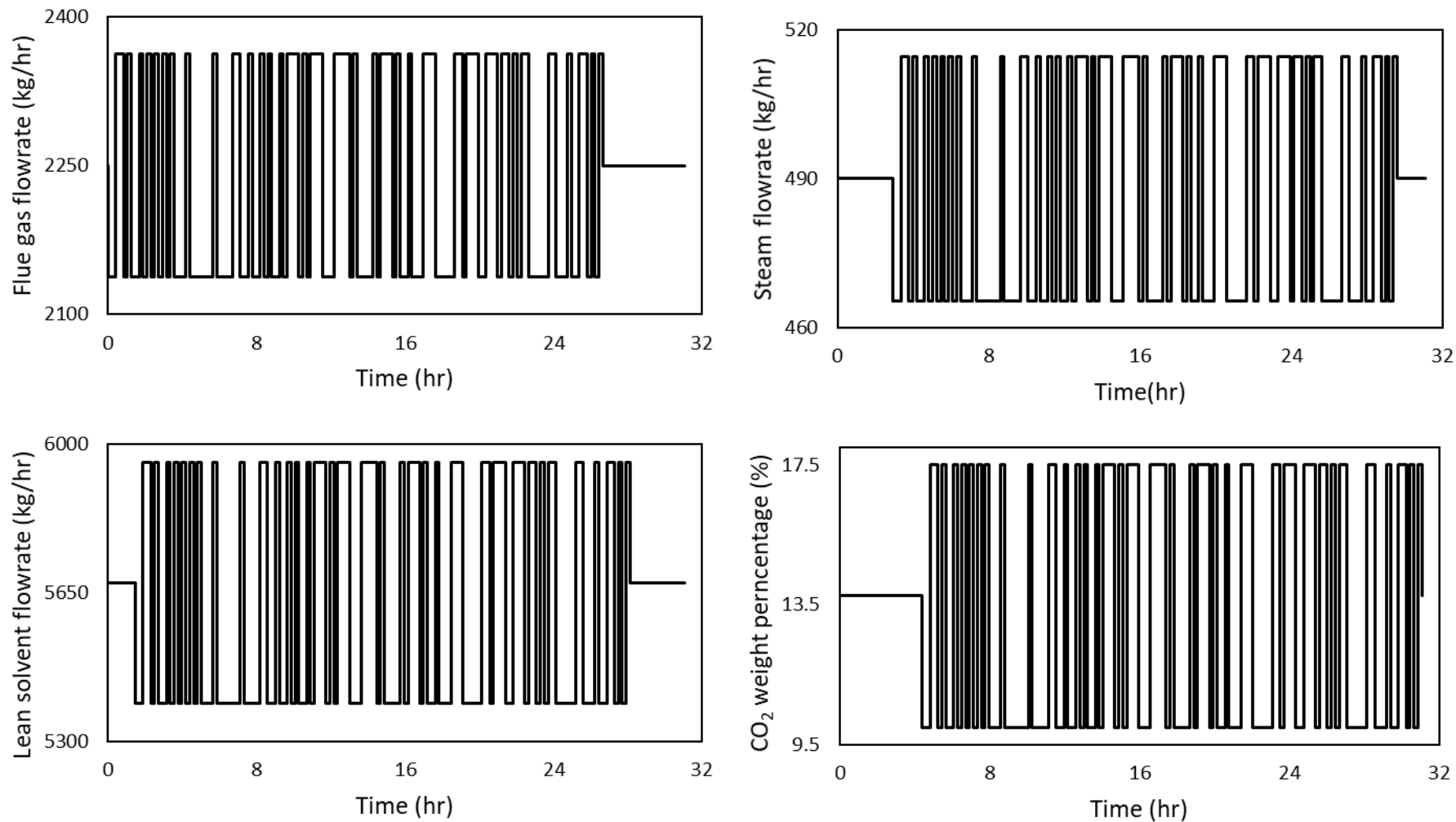


Figure 19. PRBS experiment design

Table 8. Pilot plant characteristic parameters

| Parameter | Value |
|--------------------|-------|
| n_r | 4 |
| τ_{dom}^H | 0.92 |
| τ_{dom}^L | 0.15 |
| T_{settle}^{max} | 1.44 |
| α_S | 2 |
| β_S | 3 |

The Schroeder phased experiment design is obtained by a sum of sine functions, defined as:

$$u_n(k) = \sum_{j=1}^{N_S/2} a_{[n,j]} \cos(w_j T + \phi_{[n,j]}) \quad (9)$$

with,

$$w_j = \frac{2\pi i}{N_S T} \quad (10)$$

in which n represent each of input variables and T the sampling time.

Several approaches have been used over the years for estimating the parameter matrix $a_{[n,j]}$ in Eqn 9. In this work a “zippered” design approach is used (Mart, Rivera, & Hekler, 2015). The “zippered” design defines the matrix $a_{[n,j]}$ as:

$$a_{[n,j]} = \begin{cases} 1, & j = n_r(i-1) + n \\ 0, & \text{otherwise} \end{cases} \quad (11)$$

There are also several techniques utilized to estimate the phase angle matrix $\phi_{[n,j]}$. In this work they are obtained through the minimization of the crest-factor, which influence plant friendliness while not affecting the power spectrum of the multisine signal. The crest factor (CF) is defined as the ratio of the Chebyshev norm and the l_2 -norm of the signal of each variable.

$$CF = \frac{l_\infty(u_n)}{l_2(u_n)} \quad (12)$$

The signals for the Schroeder phased input design is presented in Figure 20. The signal response obtained through the process simulation with the CCSI dynamic model is presented in Figure 21. In both Figure 20 and 21 the CO₂ capture remained constrained in between 70% and 90%, which was desired for this experiments to ensure both process stability and avoid the mass transfer pinches.

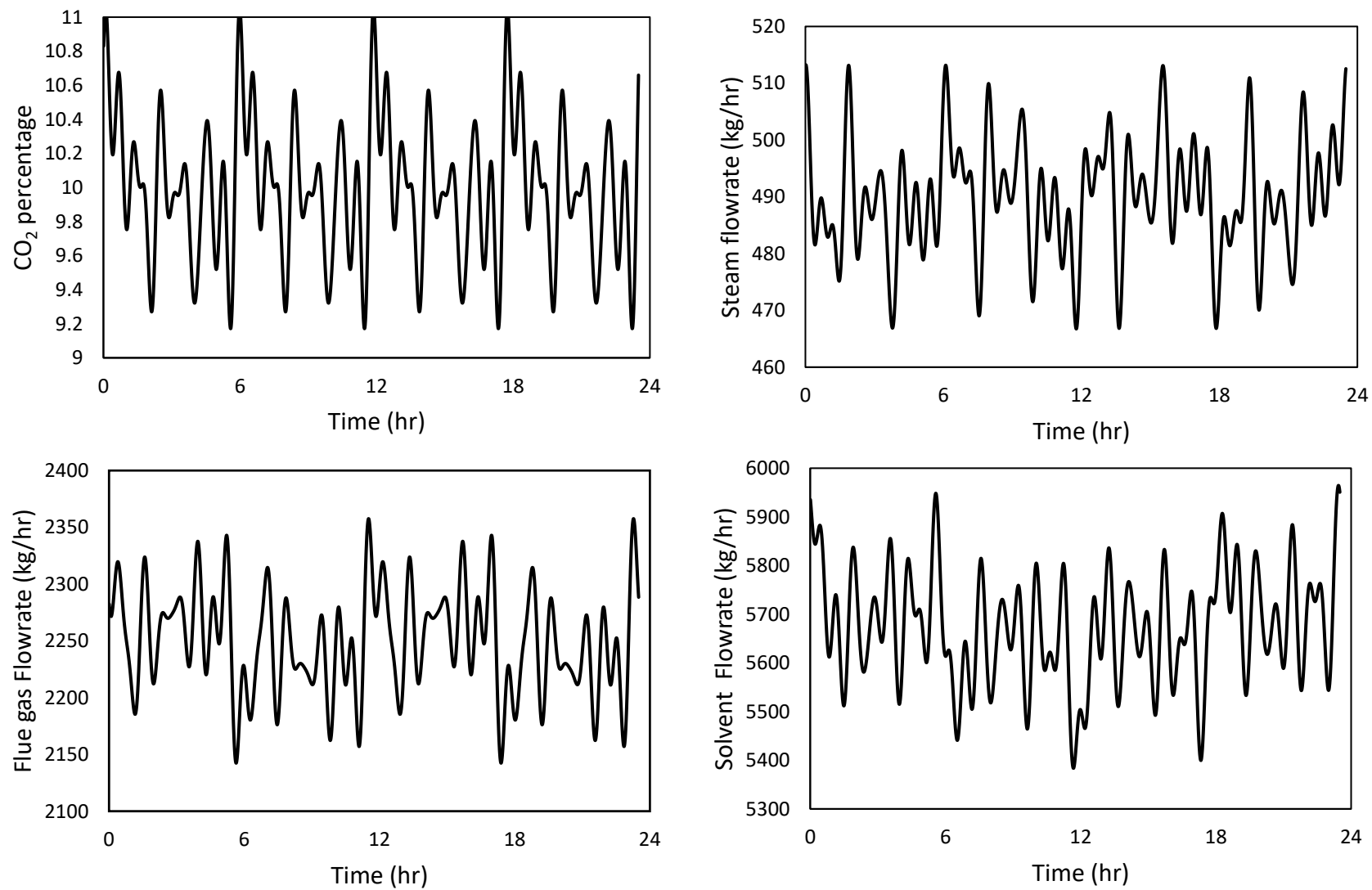


Figure 20. Schroeder phased input experiment design

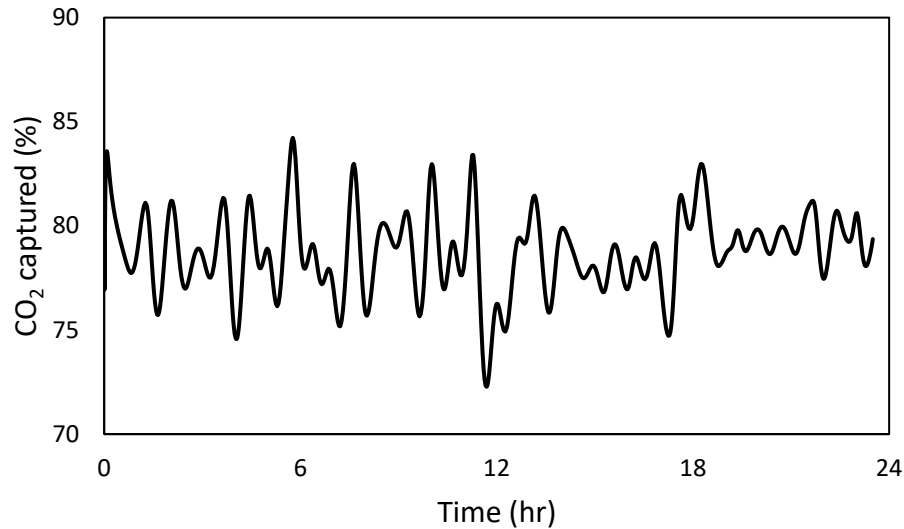


Figure 21. Schroeder phased input response signal estimation

4.2 Dynamic Data Reconciliation and Parameter Estimation

To handle missing and noisy measurements as well as mass and energy imbalances in the data, a dynamic data reconciliation (DDR) problem is solved. The methodology for the DDR has been implemented in the past (Chinen et al., 2017) for the NCCC test runs. The reconciled variables are listed below:

- Lean CO₂ loading
- Gas flow rate from absorber
- CO₂ concentration in flue gas
- Lean solvent temperature to absorber
- Lean solvent temperature from regenerator
- Lean solvent flow rate to absorber
- Flue gas flow rate
- Steam flow rate

The DDR objective function is given by equation (13)

$$\min (y_{exp} - y)' \Sigma^{-1} (y_{exp} - y)$$

s.t.

$$H(\eta, y, u, \theta) = f(\eta, y, u, \theta)$$

$$g(\eta, y, u, \theta) \leq 0$$
(13)

In the current work along with dynamic data reconciliation, a parameter estimation problem is also solved simultaneously. The parameters are related to the holdup model. Figure 22 presents the DDR results for the CO₂ capture percentage corresponding to the Schroeder phased input test runs. While the model captures the trend well, there is still discrepancy in addressing the peaks. While, further investigation is in progress, it appears that a much lower holdup volume than what is expected for the specific packing at NCCC would result in such responses. Figure 23 presents the reconciled CO₂ capture percentage for the PRBS test run. While further work is in progress, similar to the results for the Schroeder-phased inputs, there is considerable discrepancy in addressing the peaks. For the PRBS inputs, it is also observed that there are considerable realization errors in the input signals. Methodologies are being developed to address this issue such that they can be implemented within the Aspen Plus Dynamics optimization framework.

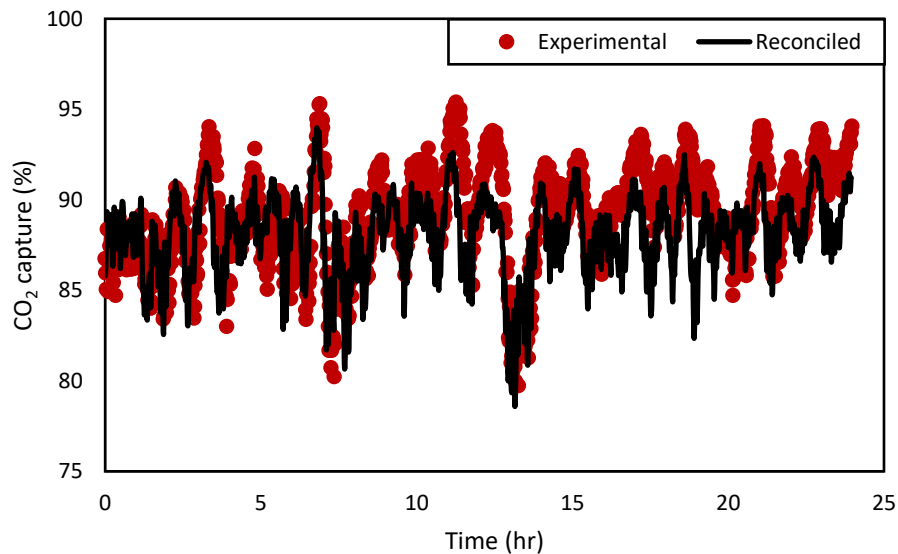


Figure 22. Reconciled Schroeder phased input results

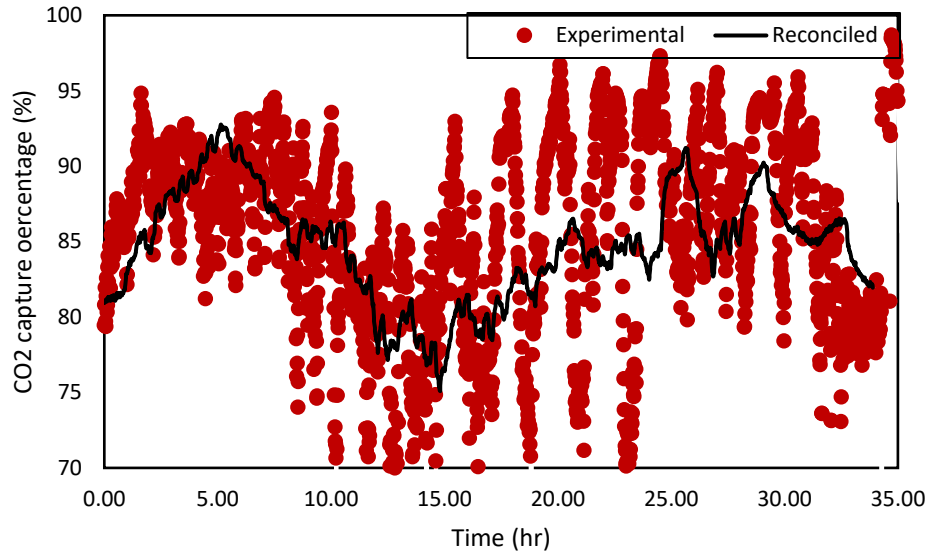


Figure 23. Reconciled PRBS results

4. CONCLUSIONS

In conclusion, a Bayesian DOE has been developed and applied to the design of a MEA solvent test campaign in the summer of 2017 at NCCC. The test campaign has been planned with the goal of constraining the CO₂ capture percentage between 50-95%, to complement the data obtained from the 2014 campaign at the same plant, for which many points were clustered above 99%. The Bayesian DOE is employed to sequentially update the test plan in light of new experimental data as they are collected. This methodology incorporates an estimate of the uncertainty of the absorber CO₂ capture percentage as a function of the model inputs (solvent and gas stream flow rates and compositions) over their ranges of interest. The prior uncertainties are estimated by propagating the submodel uncertainties (the posterior distributions from submodel UQ) through the absorber model. The test runs are chosen by an algorithm that seeks to fill the input space while selecting points for which the estimated uncertainty is relatively high. As the new data are collected, they are implemented into a Bayesian inference procedure in which the parameter distributions of the mass transfer and hydraulics models are updated while the uncertainty in the thermodynamic model parameters is kept constant. The effectiveness of this procedure in reducing the model uncertainty has been demonstrated, with an average reduction of approximately $67.2 \pm 11.6\%$ over the input space of interest, although only two iterations of sequential Bayesian DOE were ultimately performed due to limitations in time.

Although the performance of the DOE methodology has been demonstrated in this work, it is recommended that future projects focus on a more efficient, and computationally streamlined, execution of this process. An improvement in the algorithm for performing the Bayesian inference would be useful for improving the results of this project. This could be accomplished by improving the quality of the response surface model used as a surrogate for the absorber model, which could

be difficult due to the complexity of the rate-based column model. It could also be useful to develop algorithms for generating accurate surrogate models with fewer data points since evaluation of the rate-based model is computationally expensive. Alternatively, the actual model could be used for the Bayesian inference, so as to eliminate the effect of the surrogate on the accuracy of the posterior distributions obtained, although the computational expense of this method prevented its use in this work.

Two dynamic designs of experiment methodologies have been presented and successfully implemented. A dynamic data reconciliation problem was solved for the PRBS and the Schroeder phased input datasets successfully with simultaneous estimation of the holdup parameters. It is observed that the estimated parameters for the holdup models show a lower sensitivity to the liquid flow rate, density and viscosity than what was originally estimated using steady state experiments.

REFERENCES

- [1] Miller, D.C., Syamlal M., Mebane, D.S., Storlie C., Bhattacharyya D., Sahinidis N.V., Agarwal D., Tong C., Zitney S.E., Sarkar A., Sun X., Sundaresan S., Ryan E., Engel D., Dale C., 2014. Carbon capture simulation initiative: a case study in multiscale modeling and new challenges. *Annu. Rev. Chem. Biomol. Eng.* 5, 301-323.
- [2] Weaver, B.P., Williams, B.J., Anderson-Cook, C.M., Higdon, D.M., 2016. Computational enhancements to Bayesian design of experiments using Gaussian processes. *Bayesian Anal.* 11 (1), 191-213.
- [3] Morgan, J.C., Chinen, A.S., Omell, B., Bhattacharyya, D., Tong, C., Miller, D.C., 2017. Thermodynamic modeling and uncertainty quantification of CO₂-loaded aqueous MEA solutions. *Chem. Eng. Sci.* 168, 309-324.
- [4] Chinen, A.S., Morgan, J.C., Omell, B., Bhattacharyya, D., Tong, C., Miller, D.C., 2017. Development of a gold-standard model for solvent-based CO₂ capture. Part 1. Hydraulic and mass transfer models and their uncertainty quantification. (manuscript under internal review)
- [5] Rivera, D. E., Lee, H., Mittelman, H. D., & Braun, M. W. (2009). Constrained multisine input signals for plant-friendly identification of chemical process systems. *Journal of Process Control*, 19(4), 623–635.
- [6] Mart, A., Rivera, D. E., & Hekler, E. B. (2015). An Identification Test Monitoring Procedure for MIMO Systems Based on Statistical Uncertainty Estimation. *Conference on Decision and Control (CDC), (Cdc)*, 2719–2724.
- [7] Chinen, A.S., Morgan, J.C., Omell, B., Bhattacharyya, D., Miller, D.C., 2017. Development of a dynamic model for solvent-based CO₂ capture with dynamic data reconciliation from pilot plant. (manuscript in preparation)